Available online at www.sciencedirect.com
ScienceDirect
Trans. Nonferrous Met. Soc. China 29(2019) 253−262
Transactions of Nonferrous Metals Society of China
www.tnmsc.cn

Influence of high pressure and manganese addition on Fe-rich phases and mechanical properties of hypereutectic Al−Si alloy with rheo-squeeze casting

Chong LIN[1,2], Shu-sen WU[2], Shu-lin LÜ[2], He-bao WU[1], Han-xin CHEN[1]

1. Hubei Provincial Key Laboratory of Chemical Equipment Intensification and Intrinsic Safety, Wuhan Institute of Technology, Wuhan 430205, China;
2. State Key Laboratory of Materials Processing and Die & Mould Technology, Huazhong University of Science and Technology, Wuhan 430074, China

Received 3 January 2018; accepted 13 June 2018

Abstract: The influence of high pressure and manganese addition on Fe-rich phases (FRPs) and mechanical properties of Al−14Si−2Fe alloy with rheo-squeeze casting (RSC) was investigated. The semi-solid alloy melt was treated by ultrasonic vibration (UV) firstly, and then formed by squeeze casting (SC). Results show that the FRPs in as-cast SC alloys are composed of coarse β-$Al_5(Fe,Mn)Si$, δ-$Al_4(Fe,Mn)Si_2$ and bone-shaped α-$Al_{15}(Fe,Mn)_3Si_2$ phases when the pressure is 0 MPa. With RSC process, the FRPs are first refined by UV, and then the solidification under pressure further causes the grains to become smaller. The peritectic transformation occurs during the formation of α phase. For the alloy with the same composition, the ultimate tensile strength (UTS) of RSC sample is higher than that of the SC sample. With the same forming process, the UTS of Al−14Si−2Fe−0.8Mn alloy is higher than that of Al−14Si−2Fe−0.4Mn alloy.

Key words: high pressure; manganese; rheo-squeeze casting; hypereutectic Al−Si alloy; Fe-rich phases; mechanical properties

1 Introduction

In automotive industry, hypereutectic Al−Si alloys are extensively used due to their good castability, high specific strength, low expansion coefficient and excellent wear-resisting performance. They are ideal materials for producing pistons, engine blocks and cylinder liners [1,2]. Along with the increasing problem of energy and environment, engine performance is increasingly developing towards high speed, high power, low fuel consumption and low emissions. With increasing of engine speed and power, the mechanical and thermal loads that the pistons withstand are significantly increased. Adding Fe element to hypereutectic Al−Si alloys can improve the thermal stability of the alloys. However, Fe can combine with Al and Si to form coarse plate-shaped or needle-shaped Fe-rich phases (FRPs), which is detrimental to the room temperature properties of the alloys [3]. Thus, the modification of FRPs has been widespread concerned. So far, the main refinement methods of FRPs are rapid solidification [4], adding neutralizer elements (Mn, Cr) [5] and ultrasonic vibration [6−8]. The rapid solidification process mainly includes planar flow casting and spray deposition. The application of these methods has not been expanded broadly because the processing is complicated and the dimension the prepared material is limited [9]. Adding neutralizer elements to Al−Si alloys can transform the coarse plate-shaped or needle-shaped FRPs to Chinese script-shape or irregular polygon. The ratio between neutralizer element and Fe is usually not less than 0.5 [10]. However, it is not always possible to eliminate needle-shaped FRPs thoroughly [11]. Ultrasonic vibration technology has advantages such as low cost, easy operation and no pollution. The microstructure can be refined when the ultrasonic vibration is applied during the solidification of the alloy melt [12]. When the alloy melt with high iron >1 wt.% Fe is treated only by UV, the morphology of FRPs is still coarse. Moreover, the

Foundation item: Project (51605342) supported by the National Natural Science Foundation of China; Project (2015CFB431) supported by the Natural Science Foundation of Hubei Province, China; Project (K201520) supported by the Science Research Foundation of Wuhan Institute of Technology, China; Project (2016KA01) supported by the Open Research Fund Program of Hubei Provincial Key Laboratory of Chemical Equipment Intensification and Intrinsic Safety, China
Corresponding author: Chong LIN; Tel: +86-13627284232; E-mail: chonglin@wit.edu.cn
DOI: 10.1016/S1003-6326(19)64934-4

long needle-shaped FRPs cannot be completely eliminated [6−8].

In addition to alloy composition, melt treatment process and cooling rate, the pressure applied during the solidification has an important effect on the microstructure [13]. The FRPs can be refined in the conventional squeeze casting Al alloys with low iron content [14,15]. But, some needle-shaped FRPs inevitably exist in the high iron content Al alloy with conventional squeeze casting [16]. The alloys solidified under high pressure (>100 MPa) have different microstructures and properties. For example, HAN et al [17] studied the microstructure of Al−4.5Cu alloy solidified under 0.5−1.7 GPa. The results show that the size of α(Al) dendrites decreases with the increase of the pressure. DONG et al [18] investigated the microstructure of Mg−8Zn−1Y alloy solidified under high pressure. The results show that the network-shaped second phase is refined into tiny granule with the increase of pressure. The above study suggests that the solidification under high pressure can significantly refine the microstructure, and therefore improve the mechanical properties of the alloys. However, the investigations about the solidification of high iron content hypereutectic A−Si alloy under high pressure have been seldom reported. In this work, the influence of high pressure and manganese on the FRPs and mechanical properties of Al−14Si−2Fe alloy with rheo-squeeze casting is investigated. The refinement mechanism of FRPs under high pressure is also discussed.

2 Experimental

Figure 1 shows the schematic of RSC process. Figure 1(a) illustrates the schematic of the UV treatment device, which is mainly composed of ultrasonic generator, transducer and ultrasonic vibrator. The power and frequency of the UV used in this experiment are 1.6 kW and 20 kHz, respectively. The nominal compositions of the Al−14Si−2Fe (wt.%) alloys with different Mn contents are given in Table 1. The alloys used in the experiments were prepared with Al−24.45Si and Al−10Mn master alloys, pure Al, Fe, Cu, Ni and Mg. The molten metal was degassed with pure argon gas after the materials were melted in a resistance furnace. Then, a certain amount of molten aluminum was poured into a steel cup which was preheated to about 610 °C. The UV was applied on the melt when the melt was cooled down to 640 °C. The temperature range of UV is 640−620 °C and the treatment time is 90 s. After the UV was completed, the semi-solid melt was poured into the mold cavity of the squeeze casting press machine which was preheated to about 200 °C to fabricate rheo-squeeze casting (RSC) parts. The pressure was applied in both the top and bottom directions. The pressure holding time was 60 s. The diameter and height of the part obtained are 30 and 80 mm, respectively. The pressures used in the experiment were 0, 100, 200 and 300 MPa. The squeeze casting press machine is a four-column hydraulic press. The maximum displacement force is 2000 kN. For comparison, the melt without UV was poured directly at 700 °C to fabricate squeeze casting (SC) parts.

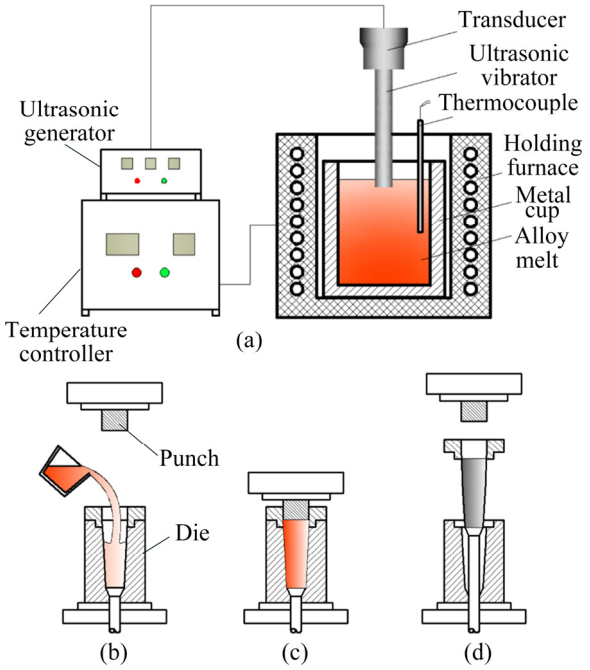

Fig. 1 Schematic of RSC process: (a) UV treatment of alloy melt; (b) Transferring melt into die cavity; (c) Closing tooling and solidifying melt under pressure; (d) Ejecting casting

Table 1 Chemical compositions of Al−14Si−2Fe alloys with different Mn contents (wt.%)

Alloy	Si	Fe	Cu	Ni	Mg	Mn	Al
M1	14	2	2	1	0.4	0.4	Bal.
M2	14	2	2	1	0.4	0.8	Bal.

A section about 10 mm in length was taken from the top of the part to prepare metallographic specimen. Then, the specimen was ground, polished and etched (with 8% sodium hydroxide). Microstructural characterization was performed using scanning electron microscope (Quanta 200 ESEM attached with EDX). The constituent phases in the alloys were determined by XRD analysis (Empyrean diffractometer). The size of the grain was determined by a metallography analysis software using statistical programs. The length of the needle-shaped or plate-shaped FRPs was measured directly. And the equivalent diameter of the grain with polyhedral morphology was determined by Heyn line intercept method:

$$D=\frac{V_f L_T}{N} \quad (1)$$

where D is the equivalent diameter of the grain, V_f is the volume fraction of the phase, L_T is the total length of the measuring line, and N is the number of the grains crossed by the measuring line. The quantitative measurement of grains in each alloy sample was conducted based on 10 optical images. Half of the SC and RSC parts were heat treated with T6 process. The T6 process was applied as follows: (1) solutionizing at 510 °C for 7 h; (2) quenching in hot water of 70−80 °C; (3) artificial aging at 190 °C for 10 h; (4) cooling in air. Then, the parts were machined to tensile samples. The schematic of the sample is shown in Fig. 2. The tensile properties were tested at room temperature by an electronic universal testing machine. Three samples for each condition were tested and an average of them was taken as the ultimate tensile strength (UTS) value.

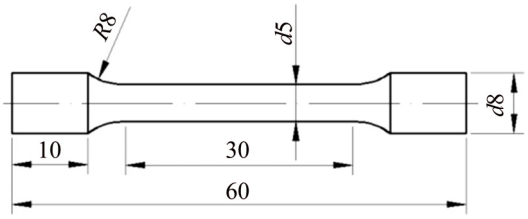

Fig. 2 Schematic of tensile samples (unit: mm)

3 Results and discussion

3.1 Microstructures of as-cast M1 and M2 alloys with SC

Figure 3 shows the microstructures of as-cast M1 alloy with SC under 0, 100, 200 and 300 MPa. The microstructure of M1 alloy is mainly composed of primary Si, eutectic structure, coarse plate-shaped δ-$Al_4(Fe,Mn)Si_2$, long needle-shaped β-$Al_5(Fe,Mn)Si$ and bone-shaped α-$Al_{15}(Fe,Mn)_3Si_2$ phases. The XRD spectra of as-cast M1 alloy with SC are shown in Fig. 4. Table 2 gives the EDX analysis results of the FRPs. According to the phase diagram, during the equilibrium solidification of Al−14Si−2Fe alloy, the primary δ phase is precipitated firstly, then the previously formed δ phase transforms into β phase through peritectic reaction $L+\delta\rightarrow\beta$+Si, and finally the eutectic structure is obtained [19]. When Mn is added into the hypereutectic Al−Si alloy with high iron content, α-$Al_{15}(Fe,Mn)_3Si_2$ phase will be formed through peritectic reaction [20].

Figure 5 shows the microstructures of as-cast M2 alloy with SC under different pressures. Similar to M1 alloy, the microstructure of M2 alloy also consists of primary Si, eutectic structure, δ, β and α phases. Figure 6 illustrates the XRD spectra of as-cast M2 alloy with SC. As can be seen from Figs. 3 and 5, with the pressure is

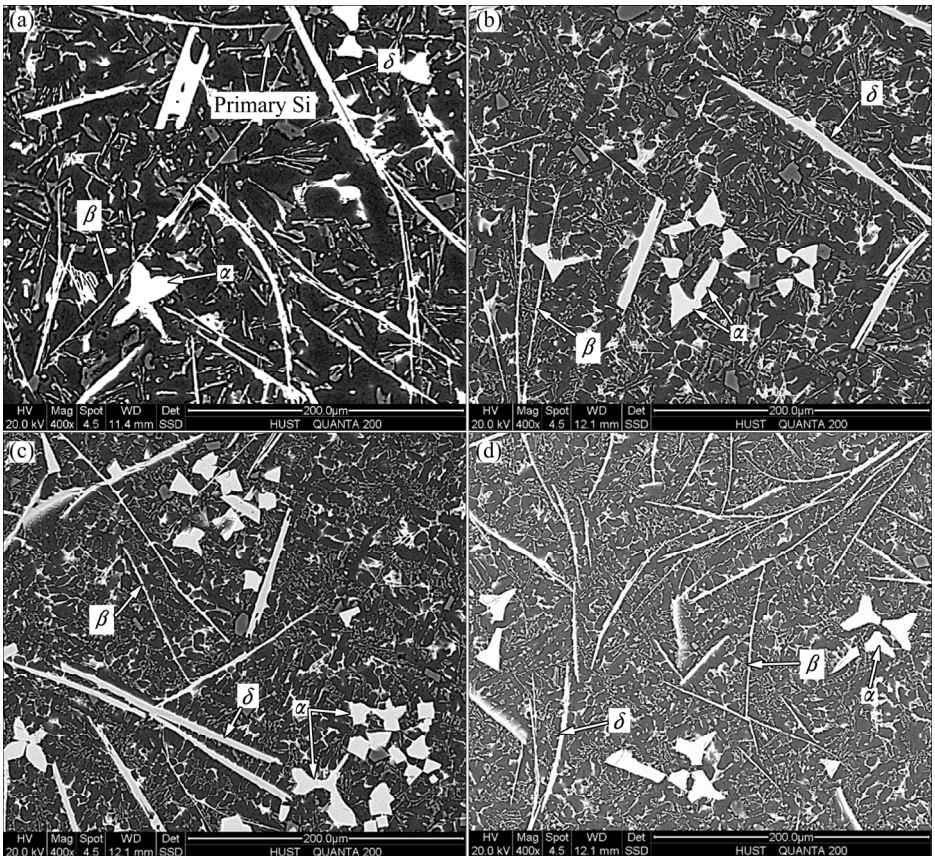

Fig. 3 Microstructures of as-cast M1 alloy with SC: (a) 0 MPa; (b) 100 MPa; (c) 200 MPa; (d) 300 MPa

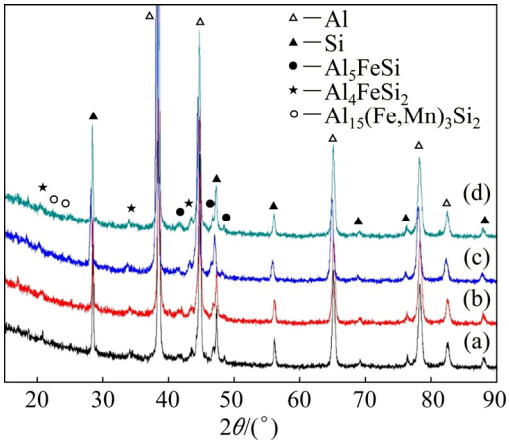

Fig. 4 XRD spectra of as-cast M1 alloy with SC: (a) 0 MPa; (b) 100 MPa; (c) 200 MPa; (d) 300 MPa

Table 2 EDX results of FRPs in as-cast M1 alloy with SC (at.%)

Phase	Al	Si	Fe	Mn
β-$Al_5(Fe,Mn)Si$	64.59	20.01	13.29	2.11
δ-$Al_4(Fe,Mn)Si_2$	51.43	31.98	14.31	2.28
α-$Al_{15}(Fe,Mn)_3Si_2$	69.51	11.73	14.44	4.32

increased from 0 to 300 MPa, the size of primary Si and eutectic structure is decreased obviously, and the size of β, δ and α phases is somewhat decreased as well. The average sizes of β, δ, α and primary Si in as-cast M1 and M2 alloy with SC at different pressures are listed in Tables 3 and 4, respectively.

3.2 Microstructures of as-cast M1 alloy with RSC

Figure 7 shows the microstructures of the as-cast M1 alloy with RSC under 0, 100, 200 and 300 MPa. The XRD spectra of the as-cast M1 alloy with RSC are shown in Fig. 8. The comparison between Figs. 8 and 4 shows that the phase constitution of M1 alloy is invariant after UV. However, the morphology of FRPs is refined obviously. Specifically, the shape of δ, β and α phase are refined into small block, short needle and irregular polygon, respectively. Moreover, with the increase of pressure, the size of δ and β phase is decreased gradually. Under 0, 100, 200 and 300 MPa, the average lengths of δ phase are about 62, 51, 43 and 36 μm, respectively. The average lengths of β phase are about 75, 60, 53 and 45 μm, respectively. The morphology of α phase also tends to be more compact and smaller as the pressure is increased.

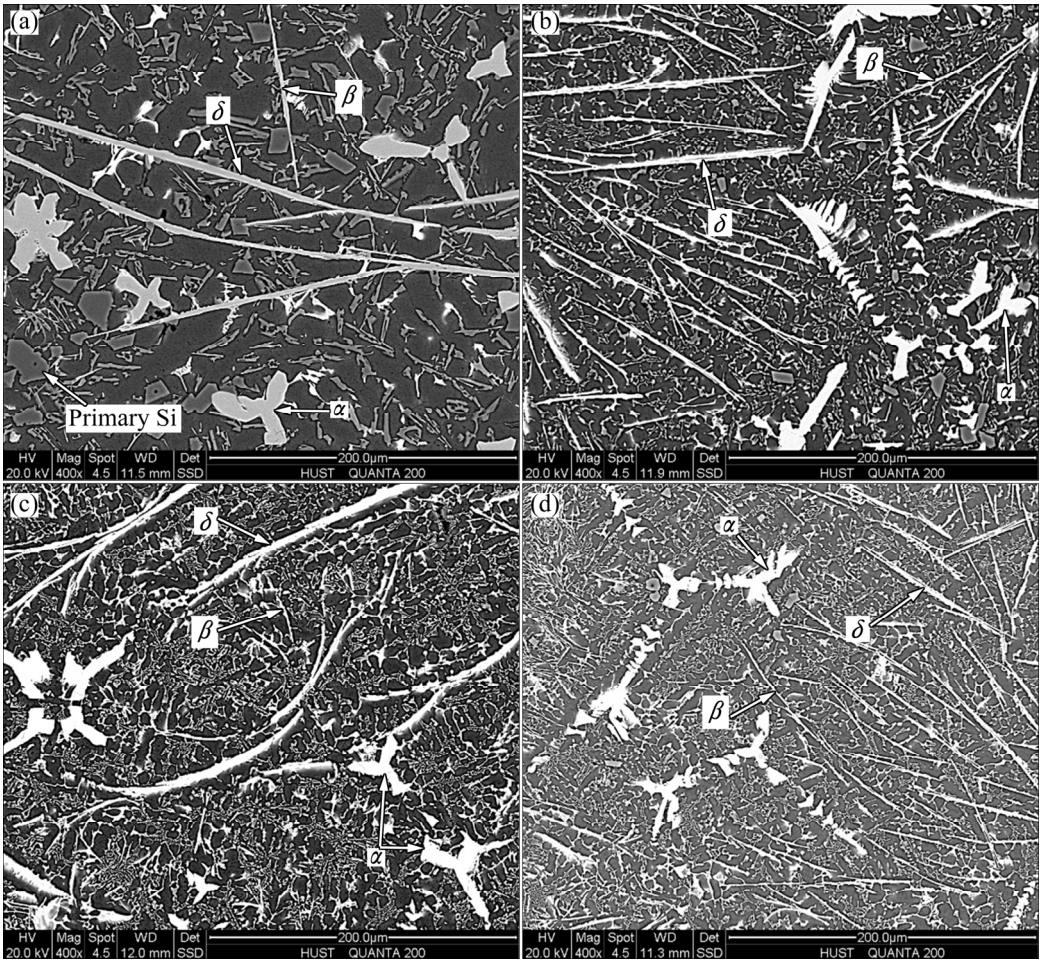

Fig. 5 Microstructures of as-cast M2 alloy with SC: (a) 0 MPa; (b) 100 MPa; (c) 200 MPa; (d) 300 MPa

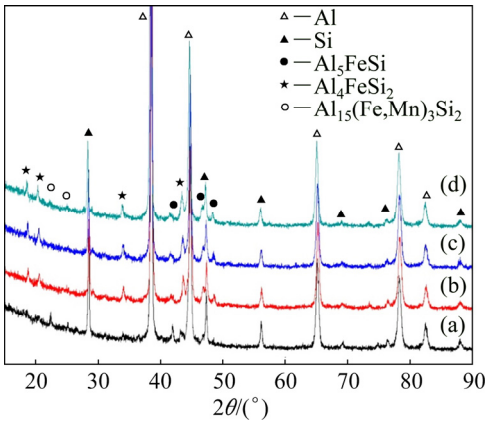

Fig. 6 XRD spectra of as-cast M2 alloy with SC: (a) 0 MPa; (b) 100 MPa; (c) 200 MPa; (d) 300 MPa

Table 3 Average size of primary phases in as-cast M1 alloy with SC

Pressure/MPa	Length of needle-shaped β phase/μm	Length of plate-shaped δ phase/μm	Equivalent diameter of α phase/μm	Equivalent diameter of primary Si/μm
0	195±60	154±46	37±8	19±3
100	178±54	143±42	32±6	15±2
200	167±51	126±37	24±5	13±1
300	151±41	112±32	21±3	12±1

Table 4 Average size of primary phases in as-cast M2 alloy with SC

Pressure/MPa	Length of needle-shaped β phase/μm	Length of plate-shaped δ phase/μm	Equivalent diameter of α phase/μm	Equivalent diameter of primary Si/μm
0	186±61	142±48	45±9	17±4
100	157±52	123±39	34±7	12±3
200	141±46	105±33	29±6	11±2
300	129±35	92±31	23±4	9±2

3.3 Peritectic transformation during formation of α phase

Figure 9 shows an enlarged SEM image of the white frame in Fig. 7(a). As can be seen, the irregular polygonal phase in the white frame has a two-layer structure, which includes the ambient gray part and the inner light part. Table 5 gives the EDX analysis results of points *A* and *B* of the phase. As can be seen, the composition of Point *A* is close to $Al_{15}(Fe,Mn)_3Si_2$. Moreover, the Mn content of Point *A* is much higher than that of Point *B*. But, the Fe content of Point *A* is less than that of Point *B*. The element distributions along the red line in Fig. 9(a) are shown in Figs. 9(b−e). It can be also observed that the Mn content of the ambient gray part is remarkably higher than that of the inner light part.

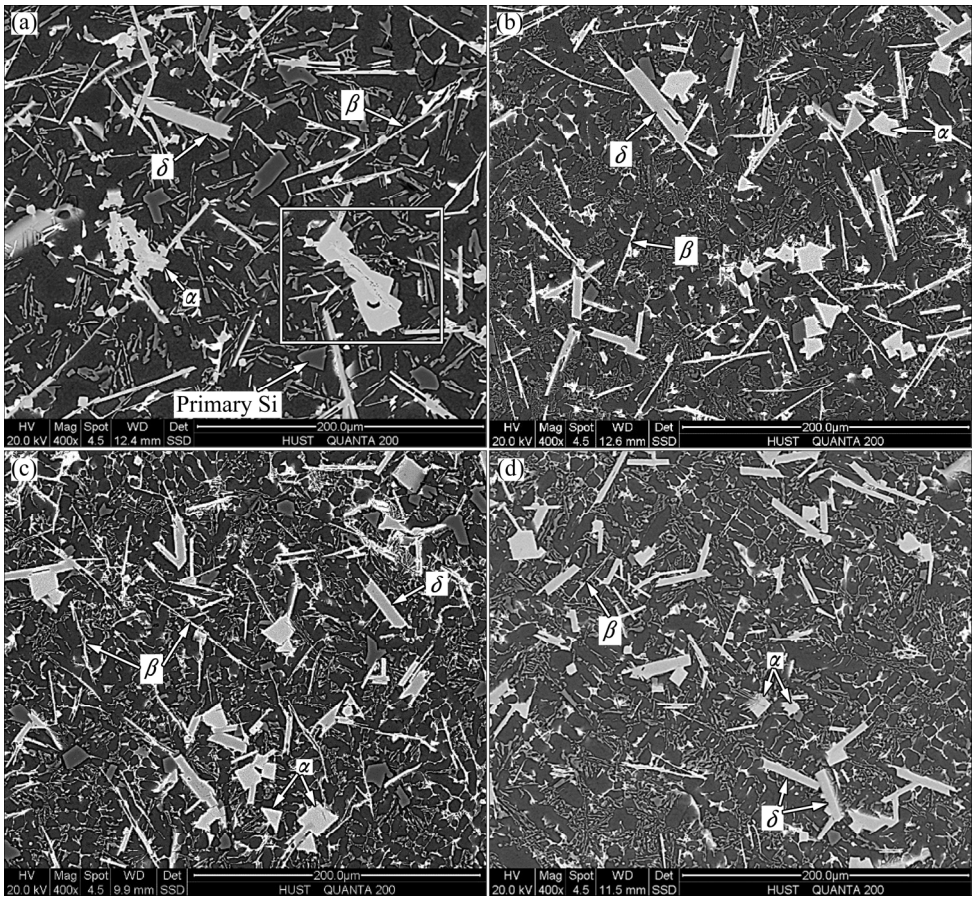

Fig. 7 Microstructures of as-cast M1 alloy with RSC: (a) 0 MPa; (b) 100 MPa; (c) 200 MPa; (d) 300 MPa

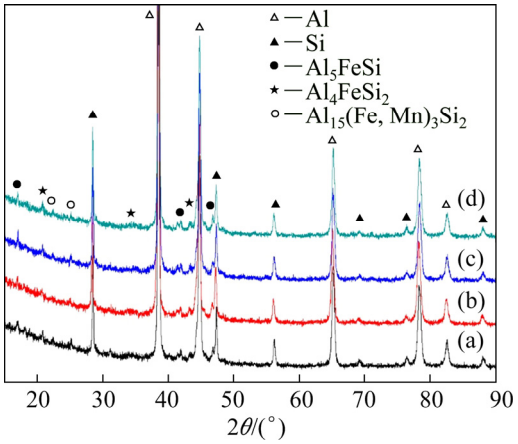

Fig. 8 XRD spectra of as-cast M1 alloy with RSC: (a) 0 MPa; (b) 100 MPa; (c) 200 MPa; (d) 300 MPa

As mentioned in Section 3.1, when Mn is added into the hypereutectic Al−Si alloy with high iron content, α-$Al_{15}(Fe,Mn)_3Si_2$ phase will be formed through peritectic reaction. The growth of α phase in peritectic alloys is classified into three stages [21]. The first is "peritectic reaction", the second is "peritectic transformation" and the third is "direct solidification". The peritectic reaction is the process that the primary phase reacts with liquid directly and peritectic phase is then formed ($L+\delta\rightarrow\alpha$). In the process of peritectic transformation, the peritectic phase is thickened by solid state diffusion ($\delta\rightarrow\alpha$). The direct solidification refers to the peritectic phase that already exists in the liquid growing directly and becoming thicker ($L\rightarrow\alpha$). The schematic diagram of three stages of peritectic reaction is shown in Fig. 10 [22]. In the first stage, the key is to

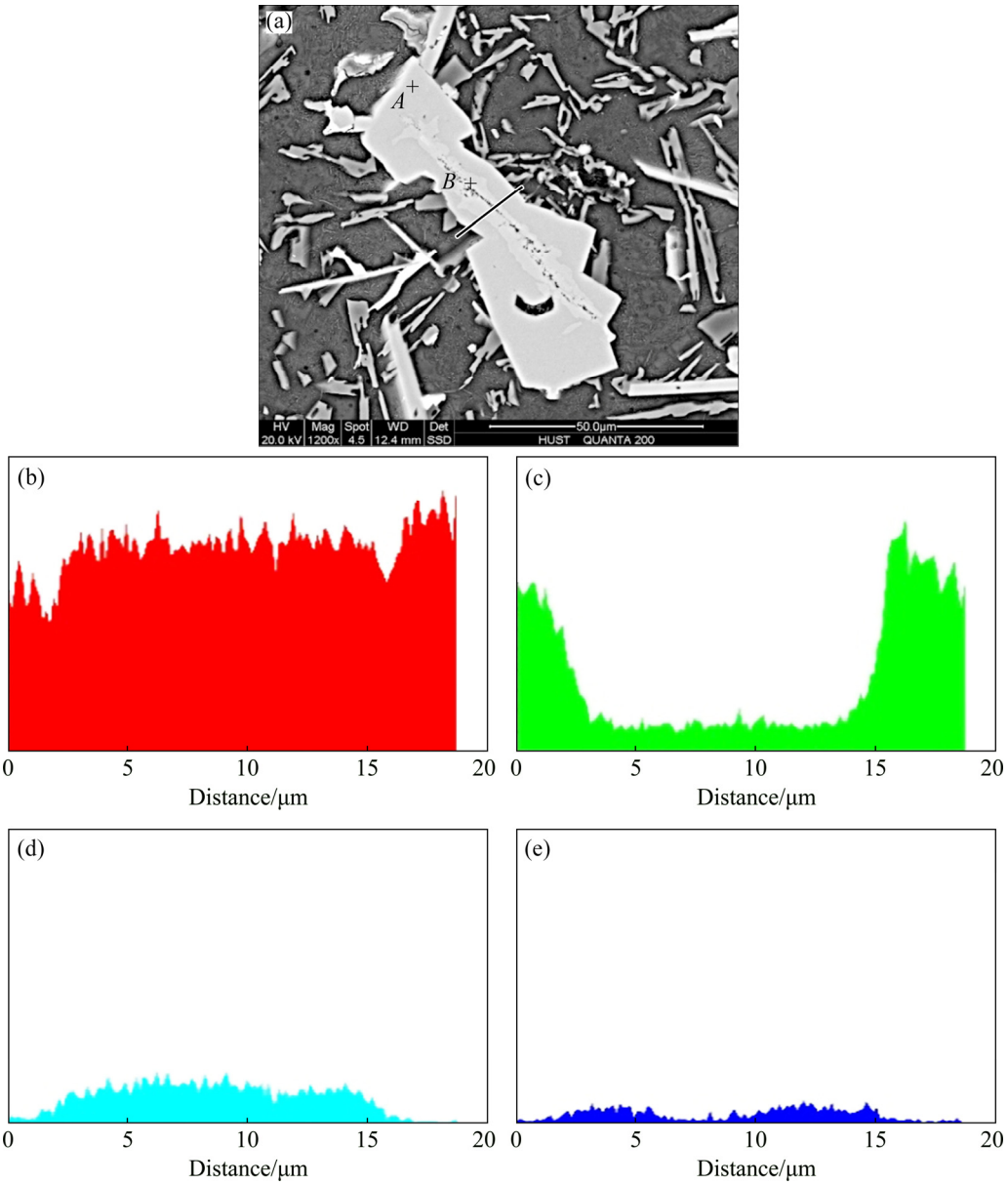

Fig. 9 Enlarged SEM image of white frame in Fig. 7(a) and distribution of elements along red line: (a) SEM image; (b) Al element; (c) Si element; (d) Fe element; (e) Mn element

Table 5 EDX analysis results of Points *A* and *B* in Fig. 9 (at.%)

Point	Al	Si	Fe	Mn
A	68.74	12.61	13.55	5.09
B	69.74	12.05	17.80	0.41

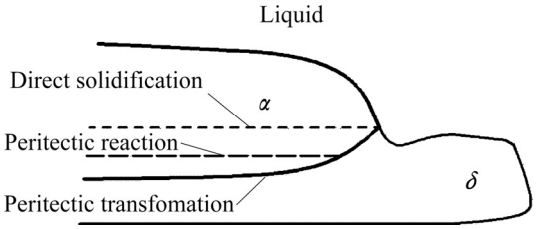

Fig. 10 Schematic diagram of three stages of growth in peritectic alloy

keep the primary phase in contact with the liquid phase. Once the primary phase is enveloped by the peritectic phase, the primary phase will be isolated. Subsequently, the peritectic reaction will be stopped. Then, the growth of the peritectic phase can only rely on the peritectic transformation and direct solidification. As can be observed in Fig. 9(a), the grey periphery of the irregular polygonal intermetallic compound is α phase, which is formed by the peritectic reaction $L+\delta\rightarrow\alpha$. Hence, the white inner part enveloped by the grey periphery can only be transformed through solid state diffusion. Namely, internal Fe atoms diffuse outwards and the external Mn atoms diffuse inwards. The composition of the interface between the peritectic phase and the liquid phase is represented by C_{α}^{L}. The composition of the interface between the peritectic phase and the primary phase is represented by C_{α}^{δ}. The driving force of the peritectic transformation through solid state diffusion is the difference between C_{α}^{L} and C_{α}^{δ} [23].

Because the size of the irregular polygonal intermetallic compound in Fig. 9(a) is large, the diffusion of the Mn and Fe element in inner and outer layers is not completed yet. Figure 11 shows the SEM image of the smaller α phase in which the process of solid state diffusion is almost finished. As can be seen, the area of white inner part of the α phase is significantly reduced compared to that in Fig. 9(a).

3.4 Microstructures of as-cast M2 alloys with RSC

Figures 12 and 13 show the microstructure and XRD spectra of the as-cast M2 alloy with RSC, respectively. Compared with the alloy with SC, the phase composition in the alloy with RSC is invariant, as can be seen in Figs. 13 and 6. In addition, the FRPs in Fig. 12 are refined remarkably. In contrast with the FRPs of M1 alloy with RSC shown in Fig. 7, most FRPs in M2 alloy with RSC have a round and granular shape, as can be seen in Fig. 12. Moreover, the amount of needle-shaped

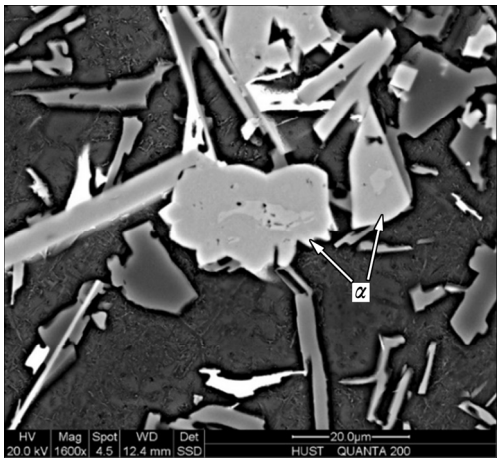

Fig. 11 SEM image of smaller α phase in as-cast M1 alloy with RSC at pressure of 0 MPa

β phase is decreased obviously in Fig. 12. This can also be confirmed by the XRD spectra. The diffraction peak of β phase in Fig. 13 is weakened obviously compared with that in Fig. 8. The ratios of Mn/Fe in M1 and M2 alloy are 0.2 and 0.4, respectively. Namely, the ratio of Mn/Fe in M2 alloy is higher than that in M1 alloy. As mentioned above, the solidification process of Al−14Si−2Fe alloy is $\delta\rightarrow\beta\rightarrow$eutectic structure. When Mn is added into the alloy, α-$Al_{15}(Fe,Mn)_3Si_2$ phase will be formed through peritectic reaction. The precipitation temperature of α phase will be raised when the Mn content is increased [24]. Therefore, more α phase will be formed when more Mn is added into the alloy. For this reason, the amounts of δ and β phase are decreased in M2 alloy. After calculation, the average equivalent diameters of the granular-shaped FRPs in Figs. 12(a−d) are about 23, 19, 14 and 12 μm, respectively. And that is to say, the size of FRPs in M2 alloy with RSC is decreased with the increase of pressure.

3.5 Refining mechanism of FRPs in alloys with RSC

The cavitating and acoustic streaming effects are generated when the ultrasound spreads inside the melt [12,25]. As a result, the shapes of δ, β and α phases are refined into small block, short needle and irregular polygon, respectively, as shown in Figs. 7(a) and 12(a).

In the RSC process, the alloy melt was treated by UV firstly and then poured into the cavity of squeeze casting press, and the solidification under pressure leads to the further refinement of FRPs, as shown in Figs. 7(b−d) and 12(b−d). On one hand, with the increase of pressure, the heat exchange coefficient between the melt and mold will correspondingly increase, thereby the cooling rate of melt is increased [26]. Hence, the solidification under pressure can decrease the grain size. On the other hand, according to the equation of Clausius−Clapeyron:

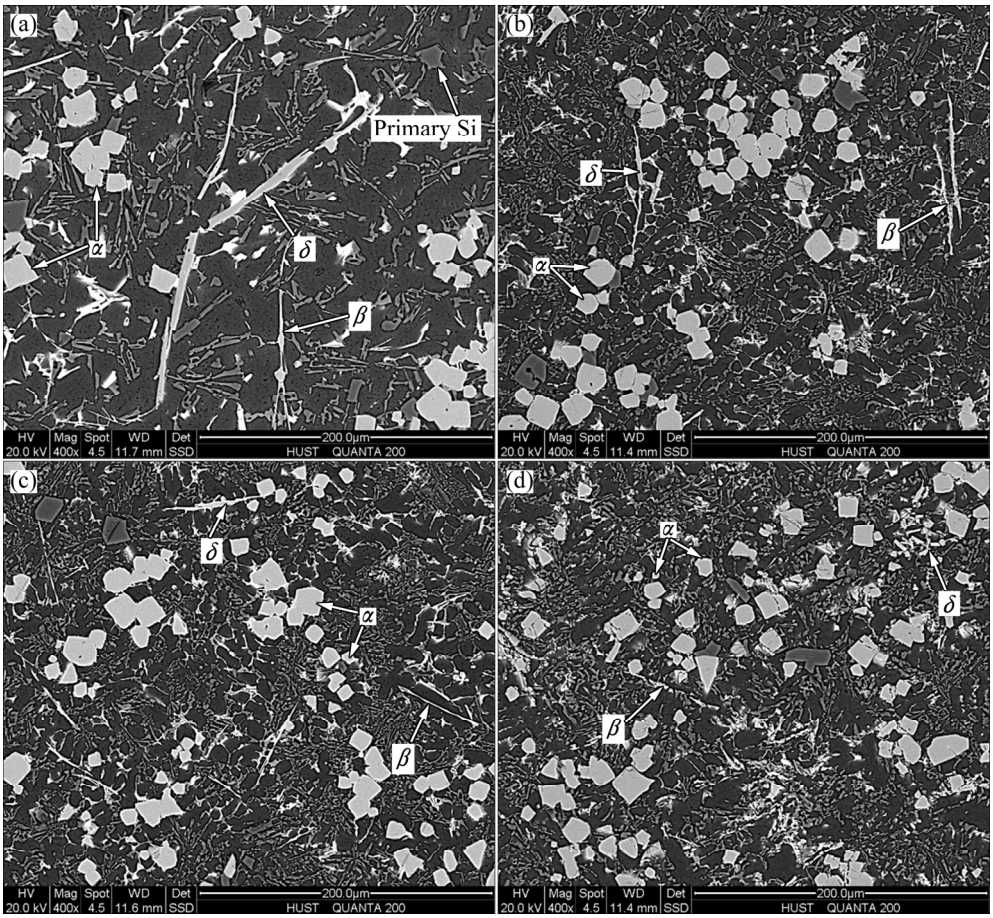

Fig. 12 Microstructures of as-cast M2 alloy with RSC: (a) 0 MPa; (b) 100 MPa; (c) 200 MPa; (d) 300 MPa

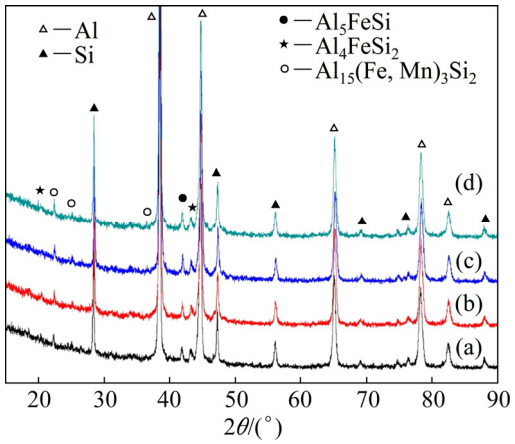

Fig. 13 XRD spectra of as-cast M2 alloy with RSC: (a) 0 MPa; (b) 100 MPa; (c) 200 MPa; (d) 300 MPa

$$\frac{\Delta T_m}{\Delta P}=\frac{T_m(V_L-V_S)}{\Delta H} \tag{2}$$

where ΔT_m is melting point variation of metal melt at high pressure, T_m is melting point of metal melt in equilibrium state, V_L is specific volume of liquid metal, V_S is specific volume of solid metal, ΔH is enthalpy change during solidification of metal melt, and ΔP is variation value of pressure. If T_m=933.3 K, V_L=0.42 m^3/kg, V_S=0.37 m^3/kg, ΔH=0.397×10^6 J/kg and ΔP=10^6 Pa, the melting point variation (ΔT_m) of pure aluminum melt at 100 MPa is 11.7 K. Because of this reason, high pressure can increase the melting point, thereby increasing the undercooling. Thus, the nucleating rate of second phase is increased. This leads to the refinement of microstructure of the alloys. Moreover, the diffusion of atoms is restrained and activation energy of the crystal growth is increased at high pressure [27]. Therefore, the growth rate of crystal will be decreased by high pressure. Due to the above reasons, the size of FRPs gets smaller gradually with the pressure increasing from 100 to 300 MPa, as shown in Figs. 7 and 12.

3.6 Mechanical properties

The mechanical properties of M1 and M2 alloys are shown in Figs. 14 and 15. As can be observed, when the composition is the same, the RSC alloy has a higher UTS compared with that of the SC alloy. Under the pressure of 0, 100, 200 and 300 MPa, the UTS of M1 alloy with RSC is increased by 20.3%, 37.1%, 34.6% and 38.6%, respectively, compared with that of the M1 alloy with SC. For M2 alloy, the UTS is increased by 33.1%, 34.0%, 32.1% and 29.4%, respectively. It is well known that the relationship between tensile strength and crystal size can

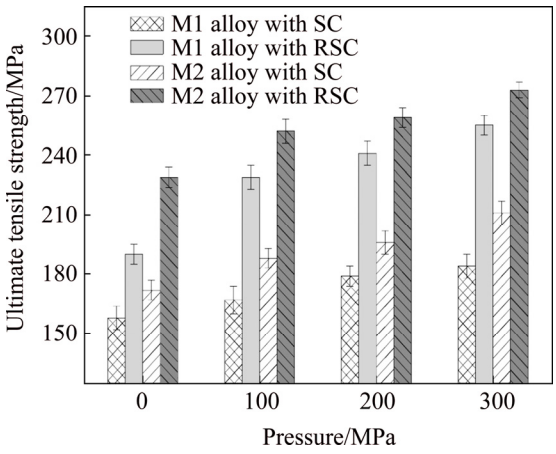

Fig. 14 UTS of M1 and M2 alloys formed with SC and RSC

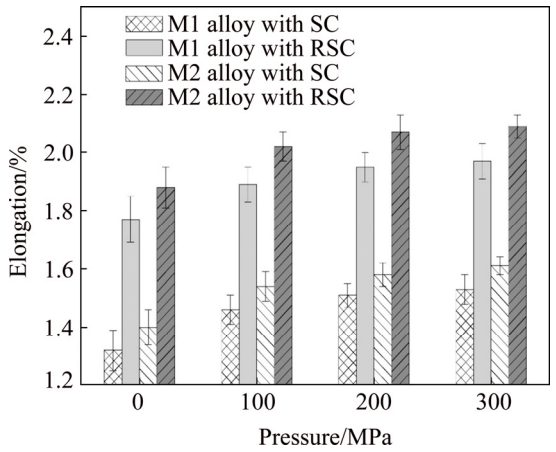

Fig. 15 Elongation of M1 and M2 alloys formed with SC and RSC

be described by the Hall−Petch formula [28]:

$$\sigma_b = \sigma_0 + kd^{-1/2} \quad (3)$$

where σ_b represents UTS, σ_0 is lattice friction, k is the Hall−Petch constant and d is the average crystal size. The microstructure of the RSC alloy is much finer than that of the SC alloy. For this reason, the UTS of the RSC alloy is increased compared to that of the SC alloy. Moreover, the UTS is increased with the increase of the pressure for both the SC and RSC alloys. As can be seen in Figs. 3(a) and 5(a), the FRPs in the SC alloys with no pressure are mainly in coarse plate shape or long needle shape. As the pressure is increased gradually, the primary Si and eutectic structure are refined obviously. The size of δ, β and α phases is somewhat decreased as well. Thus, the UTS of the SC alloy is increased with the increase of pressure. When the UV is applied, the FRPs are refined significantly, as shown in Figs. 7(a) and 12(a). With the increase of pressure, the size of FRPs in RSC alloys is further decreased, as illustrated in Figs. 7(b−d) and 12(b−d). Hence, with the increase of pressure, the UTS of the RSC alloy is also increased. Finally, the UTS of M2 alloy with 0.8% Mn is higher than that of the M1 alloy with 0.4%Mn under the same forming process. For example, with SC and under the pressure of 0, 100, 200 and 300 MPa, the UTS of M2 alloy is increased by 8.9%, 12.6%, 9.5% and 14.7%, respectively, compared with that of the M1 alloy. With RSC, the UTS of M2 alloy is increased by 20.5%, 10.0%, 7.5% and 7.1%, respectively, compared with that of the M1 alloy. The reason for this is that the addition of 0.8% Mn raises the precipitation temperature of α phase [24], thereby enlarging the phase region of α phase. As a result, the formation of fine α phase is promoted.

4 Conclusions

(1) When the pressure is 0 MPa, the FRPs of SC Al−14Si−2Fe−(0.4,0.8)Mn alloys are mainly composed of coarse β-$Al_5(Fe,Mn)Si$, δ-$Al_4(Fe,Mn)Si_2$ and bone-shaped α-$Al_{15}(Fe,Mn)_3Si_2$ phases. During the solidification of the RSC alloys, the FRPs are first refined by UV treatment, and then the size of them is further reduced as the pressure is increased from 100 to 300 MPa.

(2) The peritectic transformation occurs during the formation of α phase. The addition of 0.8% Mn promotes the formation of α phase. Under the same pressure, the FRPs in RSC Al−14Si−2Fe−0.8Mn alloy are finer and rounder than those of the RSC Al−14Si−2Fe−0.4Mn alloy.

(3) The UTS of RSC sample is higher than that of the SC sample for the alloy with the same composition. With SC and under the pressure of 0, 100, 200 and 300 MPa, the UTS of Al−14Si−2Fe−0.8Mn alloy is increased by 8.9%, 12.6%, 9.5% and 14.7%, respectively, compared with that of Al−14Si−2Fe−0.4Mn alloy. With RSC, the UTS of Al−14Si−2Fe−0.8Mn alloy is increased by 20.5%, 10.0%, 7.5% and 7.1%, respectively, compared with that of Al−14Si−2Fe−0.4Mn alloy.

References

[1] HUANG Zhi-li, WANG Kai, ZHANG Zhi-ming, LI Bo, XUE Han-song, YANG Da-zhuang. Effects of Mg content on primary Mg_2Si phase in hypereutectic Al−Si alloys [J]. Transactions of Nonferrous Metals Society of China, 2015, 25: 3197−3203.

[2] ZHENG Zhi-kai, JI Yong-jian, MAO Wei-min, YUE Rui, LIU Zhi-yong. Influence of rheo-diecasting processing parameters on microstructure and mechanical properties of hypereutectic Al−30%Si alloy [J]. Transactions of Nonferrous Metals Society of China, 2017, 27: 1264−1272.

[3] ABOUEI V, SHABESTARI S G, SAGHAFIAN H. Dry sliding wear behaviour of hypereutectic Al−Si piston alloys containing iron-rich intermetallics [J]. Materials Characterization, 2010, 61:1089−1096.

[4] HOU L G, CUI C, ZHANG J S. Optimizing microstructures of hypereutectic Al−Si alloys with high Fe content via spray forming technique [J]. Materials Science and Engineering A, 2010, 527: 6400−6412.

[5] PRŮŠA F, VOJTĚCH D. Mechanical properties and thermal stability of Al−23Si−8Fe−1Cr and Al−23Si−8Fe−5Mn alloys prepared by powder metallurgy [J]. Materials Science and Engineering A, 2013, 565: 13−20.
[6] ZHANG Yu-bo, JIE Jin-chuan, GAO Yuan, LU Yi-ping, LI Ting-ju. Effects of ultrasonic treatment on the formation of iron-containing intermetallic compounds in Al−12%Si−2%Fe alloys [J]. Intermetallics, 2013, 42: 120−125.
[7] OSAWA Y, TAKAMORI S, KIMURA T, KAZUMI M, HIDEKI K. Morphology of intermetallic compounds in Al−Si−Fe alloy and its control by ultrasonic vibration [J]. Materials Transactions, 2007, 48: 2467−2475.
[8] LIN Chong, WU Shu-sen, ZHONG Gu, WAN Li, AN Ping. Effect of ultrasonic vibration on Fe-containing intermetallic compounds of hypereutectic Al−Si alloys with high Fe content [J]. Transactions of Nonferrous Metals Society of China, 2013, 23: 1245−1252.
[9] KORAMAN E, BAYDOĞAN M, SAYILGAN S, KALKANLI A. Dry sliding wear behavior of Al−Fe−Si−V alloys at elevated temperatures [J]. Wear, 2015, 322−323: 101−107.
[10] JI Shou-xun, YANG Wen-chao, GAO Feng, WATSON D, FAN Zhong-yun. Effect of iron on the microstructure and mechanical property of Al−Mg−Si−Mn and Al−Mg−Si diecast alloys [J]. Materials Science and Engineering A, 2012, 564: 130−139.
[11] COUTURE A. Iron in aluminium casting alloys—A literature survey [J]. AFS International Cast Metals Journal, 1981, 6: 9−17.
[12] ESKIN G I. Influence of cavitation treatment of melts on the processes of nucleation and growth of crystals during solidification of ingots and castings from light alloys [J]. Ultrasonics Sonochemistry, 1994, 1: s59−s63.
[13] MALEKI A, SHAFYEI A, NIROUMAND B. Effects of squeeze casting parameters on the microstructure of LM13 alloy [J]. Journal of Materials Processing Technology, 2009, 209: 3790−3797.
[14] ZHANG Wei-wen, LIN Bo, ZHANG Da-tong, LI Yuan-yuan. Microstructures and mechanical properties of squeeze cast Al−5.0Cu−0.6Mn alloys with different Fe content [J]. Materials and Design, 2013, 52: 225−233.
[15] DONG J X, KARNEZIS P A, DURRANT G, CANTOR B. The effect of Sr and Fe additions on the microstructure and mechanical properties of a direct squeeze cast Al−7Si−0.3Mg alloy [J]. Metallurgical and Materials Transactions A, 1999, 30: 1341−1356.
[16] ARHAMI M, SARIOGLU F, KALKANLI A, HASHEMIPOUR M. Microstructural characterization of squeeze-cast Al−8Fe−1.4V−8Si [J]. Materials Science and Engineering A, 2008, 485: 218−223.
[17] HAN Y S, KIM D H, LEE H I, KIM Y G. Effect of applied pressure during solidification on the microstructural refinement in an Al−Cu alloy [J]. Scripta Metallurgica et Materialia, 1994, 31: 1623−1628.
[18] DONG Yun, LIN Xiao-ping, XU Rui, ZHENG Run-guo, FAN Zhi-bin, LIU Shi-jun, WANG Zhe. Microstructure and compression deformation behavior in the quasicrystal-reinforced Mg−8Zn−1Y alloy solidified under super-high pressure [J]. Journal of Rare Earths, 2014, 32: 1048−1055.
[19] MONDOLFO L F. Aluminum alloys: Structure and properties [M]. London: Butterworths, 1976: 283−536.
[20] BELOV N A, AKSENOV A A, ESKIN D G. Iron in aluminum alloys: Impurity and alloying element [M]. London: Taylor & Francis, 2002: 116−118.
[21] KERR H W, KURZ W. Solidification of peritectic alloys [J]. International Materials Reviews, 1996, 41: 129−164.
[22] LI Shuang-ming, LU Hai-yan, LI Xiao-li, LIU Lin, FU Heng-zhi. Directional solidification and growth of peritectic alloys [J]. Rare Metal Materials and Engineering, 2005, 34: 234−239.
[23] JOHN D H S, HOGAN L M. A simple prediction of the rate of the peritectic transformation [J]. Acta Metallurgica, 1987, 35: 171−174.
[24] KIM H Y, PARK T Y, HAN S W, LEE H M. Effects of Mn on the crystal structure of α-Al(Mn,Fe)Si particles in A356 alloys [J]. Journal of Crystal Growth, 2006, 291: 207−211.
[25] ESKIN G I, MAKAROV G S, PIMENOV Y P. Effect of ultrasonic processing of molten metal on structure formation and improvement of properties of high-strength Al−Zn−Mg−Cu−Zr alloys [J]. Advanced Performance Materials, 1995, 2: 43−50.
[26] GHOMASHCHI M R, VIKHROV A. Squeeze casting: An overview [J]. Journal of Materials Processing Technology, 2000, 101: 1−9.
[27] WEI Z J, WANG Z L, WANG H W, CAO L. Evolution of microstructures and phases of Al−Mg alloy under 4 GPa high pressure [J]. Journal of Materials Science, 2007, 42: 7123−7128.
[28] VEPŘEK S. The search for novel, superhard materials [J]. Journal of Vacuum Science & Technology A, 1999, 17: 2401−2420.

高压和锰添加对流变挤压成形过共晶 Al−Si 合金富铁相和力学性能的影响

林 冲[1,2]，吴树森[2]，吕书林[2]，吴和保[1]，陈汉新[1]

1. 武汉工程大学 化工装备强化与本质安全湖北省重点实验室，武汉 430205；
2. 华中科技大学 材料成形与模具技术国家重点实验室，武汉 430074

摘 要：研究高压和锰添加对流变挤压成形 Al−14Si−2Fe 合金富铁相和力学性能的影响。首先，将半固态合金熔体进行超声振动处理，然后挤压成形。结果显示，当挤压力为 0 MPa 时，无超声挤压成形的 Al−14Si−2Fe−(0.4,0.8)Mn 合金铸态组织中的富铁相主要由粗大 β-$Al_5(Fe,Mn)Si$ 相、δ-$Al_4(Fe,Mn)Si_2$ 相和骨骼状 α-$Al_{15}(Fe,Mn)_3Si_2$ 相组成。在流变挤压成形下，富铁相首先被超声振动细化，然后压力下的凝固使其尺寸进一步减小。在 α 相的形成过程中发生包晶反应。当合金成分相同时，流变挤压成形试样比无超声挤压成形试样的抗拉强度高；当成形工艺相同时，Al−14Si−2Fe−0.8Mn 合金比 Al−14Si−2Fe−0.4Mn 合金的抗拉强度高。

关键词：高压；锰；流变挤压成形；过共晶 Al−Si 合金；富铁相；力学性能

(Edited by Bing YANG)